AIAA JOURNAL
Vol. 47, No. 3, March 2009

Computational-Fluid-Dynamics-Based Kriging Optimization Tool for Aeronautical Combustion Chambers

F. Duchaine,* T. Morel,† and L. Y. M. Gicquel‡
Centre Européen de Recherche et de Formation Avancée en Calcul Scientifique, 31057 Toulouse, France

DOI: 10.2514/1.37808

The current state of the art in computational fluid dynamics provides reasonable reacting-flow predictions and is already used in industry to evaluate new concepts of gas turbine engines. In parallel, optimization techniques have reached maturity and several industrial activities benefit from enhanced search algorithms. However, coupling a physical computational fluid dynamics model with an optimization algorithm to yield a decision-making tool needs to be undertaken with care to take advantage of the current computing power while satisfying the gas turbine industrial constraints. Among the many delicate issues for such tools to contribute efficiently to the gas turbine industry, combustion is probably the most challenging, and optimization algorithms are not easily applicable to such problems. In our study, a fully encapsulated algorithm addresses the issue by making use of a new multiobjective optimization strategy based on an iteratively enhanced metamodel (kriging) coupled to a design-of-experiments method and a fully parallel three-dimensional computational fluid dynamics solver to model turbulent reacting flows. With this approach, the computer cost needed for thousands of computational fluid dynamics computations is greatly reduced while ensuring an automatic error reduction of the approximated response function. Preliminary assessments of the search algorithm against simple analytical test functions prove the strategy to be efficient and robust. Application to a three-dimensional industrial aeronautical combustion chamber demonstrates the approach to be feasible with currently available computing power. One result of the optimization is that possible design changes can improve performance and durability of the studied engine. With the advent of massively parallel architectures, the intersection between these two advanced techniques seems a logical path to yield fully automated decision-making tools for the design of gas turbine engines.

Nomenclature

$f(X)$	=	objective function of optimization parameters X
$\hat{f}(X)$	=	approximation of $f(X)$
f_M	=	merit function
$\dot{m}_a$	=	air mass flow entering the primary zone
P	=	pressure
P_{dt}	=	airflow split between the swirler and the multiperforated plates
P_{mp}	=	airflow split between external and internal multiperforated plates
P_{pi}	=	position of primary jets
Pr_f^s	=	stator thermal stress criterion
Q	=	mass flow rate
S	=	surface
T	=	temperature
V	=	velocity
V_c	=	volume of the primary zone
X	=	set of optimization parameters
$X^\star$	=	global optimum parameters
η_c	=	combustion efficiency
θ	=	parameter of the combustion efficiency
ρ	=	flow density
ϱ	=	parameter of the merit function
σ	=	porosity of multiperforated plates
$\hat{\sigma}_f(X)$	=	variance of the approximation $\hat{f}(X)$
Φ_β	=	criterion of spatial homogeneity of samples in a design space

Subscripts

MP	=	multiperforation value
T	=	swirler value
3	=	compressor value
4	=	plane 4 value

Superscripts

a	=	dimensionless value
b	=	baseline value
e	=	external value
i	=	internal value
ref	=	reference value

I. Introduction

SYSTEMATIC use of optimization for gas turbine combustion chambers is usually limited due to the substantial computing power required by such applications. Furthermore, global optimization strategy remains beyond today's limits, and well-tuned, targeted search methods (based on know-how) in a restrained design space are the only viable options. Despite these constraints, numerous domains have seen the advent of fully automated decision-making tools to help the design of new devices. In fluid mechanics, contributions remain quite limited because of the difficulty in obtaining accurate flow estimates and the need for highly-computer-demanding algorithms. Flow predictions in real applications are usually obtained by computational fluid dynamics (CFD), which necessitate the numerical solution of spatially and temporally dependent partial differential equations. The resolution of this system of equations usually takes 4–5 h on modern supercomputers. That nonnegligible computational effort accentuates the need for

Received 31 March 2008; revision received 26 November 2008; accepted for publication 27 November 2008.

*Postdoctoral Student, Computational Fluid Dynamics Combustion Team, 42 Avenue Gaspard Coriolis.
†Researcher Engineer, Global Change Team, 42 Avenue Gaspard Coriolis.
‡Senior Researcher, Computational Fluid Dynamics Combustion Team, 42 Avenue Gaspard Coriolis.

intensive computing facilities, especially if optimization is targeted. It also underlines the necessity for very efficient search procedures such as gradient methods using adjoint CFD solvers [1]. Availability of the adjoint CFD solver partly explains why CFD-based optimization is mostly developed for purely aerodynamic problems [2,3], in which the maturity of the CFD codes allows access to the adjoint solvers. Recent applications of such optimization tools to 3-D aerodynamic problems have been realized [4–7] with success.

A direct application of aerodynamic-oriented techniques to fully turbulent reacting flows is not trivial. Indeed, the extended physics implied by turbulent reacting flows involve strong couplings between combustion, mixing, and flow dynamics, which makes the development of CFD adjoint solvers a difficult task. Gradient estimations can still be obtained by finite difference techniques. However, this approach is known to be sensitive to the noise generated by the numerical solution of the system, the grid management, and all the various transformations introduced by the optimization process [8]. Direct deterministic search methods [9] are therefore preferred. The primary reasons are their reliability, ease of implementation, and applicability to nonlinear and nondifferentiable problems, for which they yield good results when sophisticated approaches fail [10]. These methods are also easy first choices before going into the development of more complex approaches. They are also available in most optimization tools (i.e., Nimrod/O [11,12], DAKOTA [13], CONDOR [14], OPT + + [15], iSIGHT [16], and Optimus [17]).

In the context of optimization, algorithm design is faced with two conflicting criteria. *Exploration* indicates the capability of a method to search global interesting configurations over the whole design space. In contrast, *exploitation* indicates the capability of using already known information to rapidly converge to a local optimum. Among the deterministic approaches, zero-order models are usually limited to local searches while performing an efficient exploitation of the available data to converge rapidly to an optimum in the neighborhood of the starting point. Exploration remains critical if a global optimum is targeted. Stochastic processes are usually introduced to extend the local search by random identification of several initial search points [18]. Genetic algorithms are the most commonly used stochastic methods [8,19–21]. Finally, the coupling of efficient gradient approaches with stochastic methods would ensure efficient local and global searches [22].

As pointed out initially, the most important constraint for the development of CFD-based optimization tools is the limitation on CPU resources: the tool should provide an acceptable response time, even with CPU-demanding applications, while respecting industrial constraints. For example, the N3S-Natur CFD code needs approximately four wall-clock hours to provide a flowfield estimate in a single-sector helicopter combustion chamber. For that specific reason and because most of the cited optimization methods require multiple evaluations of the objective functions, a reduced-fidelity model [23] is introduced to limit the number of expensive CFD runs. The primary idea with this approach is to model the optimization function by an estimate based on a limited number of expensive CFD evaluations, thereby decreasing the overall CPU effort and elapsed time. With the algorithm developed in this work and in contrast to conventional approaches, the response surface model is iteratively improved to limit the errors introduced with the estimate. The enhancement of the database on which the approximation is based is obtained through automatic requests for new CFD-based evaluations, which thus provide a set of considered exact values of the response function. Note that the new method has the advantage of not requiring any CFD adjoint solver and is directly applicable to turbulent reacting-flow configurations, as targeted in this work. Similar simpler kriging-based strategies are adopted by other researchers [24] and prove to be quite successful in their own areas of application.

When faced with industrial problems, engineers have to deal with multiobjective optimization [25], and the most appropriate approach consists of providing Pareto optima to ease decision-making [26–29]. For those types of optimization problems, access to the optimal solutions is of greatest interest to the designer. However, it should not prevent identifying the tendencies and dependencies of the design to critical parameters that are valuable information for future developments. The design of experiments (DOE) in that case is mandatory to efficiently sample the design space [30,31] and provide efficient analyses of the data [32]. With the approach presented, that specificity is automatically addressed, because the fully automated decision-making tool is essentially dedicated to the improvement of the DOE. Indeed, a DOE is used to construct the estimator (kriging) that gives access to a local uncertainty on the estimate. This uncertainty is thus optimized by locally refining the DOE with new CFD evaluations.

The document is organized as follows. Specific issues pertaining to the tool automation, the code management, and the optimization algorithm are detailed in Secs. II.A–II.C and III, respectively. Verifications and illustration of the impact of the relevant optimization parameters are presented and discussed in Sec. IV.A. Finally, an application to a 3-D single sector of a real combustion chamber (Sec. IV.B) is analyzed to illustrate the applicability of the procedure to an industrial case. It results from the demonstration that new design points can be proposed to improve performance and durability of the studied engine.

II. Parameterization of CFD and Optimization Algorithms

Optimization requires the definition of control parameters determining the search space over which the studied configuration has to be improved. In the aeronautical context, the set of design parameters is very large and cannot be used as a whole. For simplicity, only geometrical and inflow conditions are chosen as possible optimization criteria. That is, a given combustion chamber is improved by acting on a limited set of parameters and is not totally designed from scratch. The user defines cost functions on the search space to assess the quality of a given design in that space. All the state variables and the functions are evaluated from CFD runs. In practice, the steps needed for the preparation of a CFD run are linked to the mathematical formulation of a fluid mechanics problem: defining the flow domain, enforcing the initial and boundary conditions, and evaluating the solution for the given set of model equations. A CFD run is hence decomposed in three phases:

1) Preprocessing includes automatic mesh generation when shape optimization is concerned, initialization of the physical fields, and determination of the boundary conditions.

2) CFD computation gives the solution of the turbulent reacting model equations.

3) Postprocessing is the automatic analysis of the CFD predictions for evaluation of the designs and optimization.

The integration of CFD in an automatic strategy for an optimization tool requires encapsulating these three steps in an efficient and robust package with limited user inputs. Some elements concerning the pre- and postprocessing phases are given subsequently. Particularities related to the optimization itself are detailed in Sec. III.

The turbulent reacting CFD code used to provide the flow prediction of the aeronautical combustion chambers is N3S-Natur. It is based on a Reynolds-averaged Navier–Stokes approach and determines the mean stationary flow features for two-phase turbulent reacting flows in complex geometries using tetrahedral grids. Details on the turbulent closures, the turbulent combustion models, and the two-phase flow solver are available in [33]. For our work, the following options are used: an implicit solver based on a Gauss–Siedel inversion (first order in time with local time-stepping) with a MUSCL second-order spatial scheme making use of a van Leer limiter. The turbulence model is the standard k-ε closure. The turbulent combustion closure is the combustion-limited-by-equilibrium model [34,35]. If dealing with two-phase reacting flows, as encountered for the real burner application, a Lagrangian model is activated and coupled to the CFD solver. Convergence of the CFD solver is based on flux balances for mass, total enthalpy, and kinetic energy. The CFD solution is thus obtained when all flux balance estimates reach values strictly below 1% of the previous

estimate. That stop criterion is used for all of our computations unless specified otherwise. Evaluations of the impact on the optimization predictions of that specific criterion were assessed and found to be weak as long as all balances were below that critical value. Validation and verification of the CFD code can be found in [34,35].

A. CFD Preprocessing

With the initial combustion chamber design being provided, the computational-domain description is assumed to be available through the computer-aided-design parameterization [36–40]. Therefore, automation of the initial and subsequent computational meshes is not addressed in detail. Only mesh quality is discussed because it is known to be a critical point when solving partial differential equations using numerical methods [41]. Indeed, great care must be taken to generate a computational grid that ensures meaningful CFD predictions. In the context of geometrical optimization, which involves transformations of an initial computational domain, two methods have been implemented and tested. The first one, generally named the moving-mesh technique [42–45], consists of updating an existing discretization to meet the new set of geometrical parameters. It simply means adjusting the initial grid node positions to fit the new design. Although this method is rather simple to implement, it is limited to small control-parameter variations to guarantee acceptable mesh qualities. The second technique aims at fully or partially regenerating a new grid for the new given set of geometrical parameters. Once the geometrical parameterization and regeneration processes are well controlled, this method offers numerous possibilities to produce good-quality grids, even for complex configurations [46–48]. For the present work, the full regeneration technique is preferred.

The initialization of the physical fields for a given computational domain is also of practical importance. It has a great influence on the time taken by the CFD computation to reach convergence (the only time when the prediction is meaningful and can be postprocessed). For our approach, interpolations based on first-order spatial Taylor developments are used to project the baseline fields on the new grids. Finally, and for most problems, adjustment of the boundary conditions to meet the specified control parameters is trivial.

B. CFD Postprocessing

Postprocessing steps are of two types in our optimization process. First, it is used to verify the flow prediction provided by the CFD code (i.e., to discriminate unphysical solutions potentially obtained with the CFD solver). These verifications are performed through the evaluation of several mass and energy balances as well as analyses of extreme physical quantities. Second, once verified, the CFD results are processed to evaluate cost functions for the given values of the control parameters. For the specific problems addressed here, these objective-function values are computed using local, planar, and/or volumetric diagnostics which are easily obtained by manipulation of the CFD prediction and its computational grid.

C. Management of the Integrated Optimization Platform

The fully encapsulated tool is composed of two main components: a) the optimizer and b) the CFD sequences which seek a prediction/approximation of the turbulent reacting flow. Both components are themselves divided in fundamental sequences corresponding to mathematical or geometrical operations and which often rely on specific computer codes. The first consequence of that multicode environment is the need for an efficient management technique of all the components (some of which are parallelized) as well as the execution of some of the components themselves in parallel. At the same level of importance, one notes the need for an efficient management of the data transfers between elements to ensure a robust and flexible tool. The use of a coupling device is retained to satisfy, at best, all of these prerequisites. The dynamic parallel code coupler PALM [49] offers such capabilities and the optimization platform which results from the present developments is based on this device. Within PALM, the application is decomposed in independent units allowing nonhierarchical coding: the different units can be launched competitively or successively according to the general algorithm and units exchange data by parallel MPI protocols (Fig. 1). The optimization application, called MIPTO (Management of an Integrated Platform for Automatic Optimization), directly inherits from these capabilities and takes advantage of high-performance computing (HPC) through the use of parallel units (i.e., parallel CFD codes) and simultaneous tasks (i.e., simultaneous CFD evaluations) management. The efficient CPU management with a device such as PALM also justifies the optimization methods as detailed subsequently. Note that no disk access is necessary as dynamic addressing is fully managed for data transfer between codes/units. If remeshing techniques necessitate a commercial software (i.e., GAMBIT [50] in the coming example), MIPTO is able to send requests to check for license availability. That software may be accessed on a distant server if not available where the application is operating. Details about the developed and implemented methods in MIPTO can be found in [51].

III. Optimization Process

The optimization methodology is constructed to do the following:

1) Provide relationships between control variables and objective functions (mean tendencies, relative importance of optimization parameters).

2) Inform about local and global optima for each objective function.

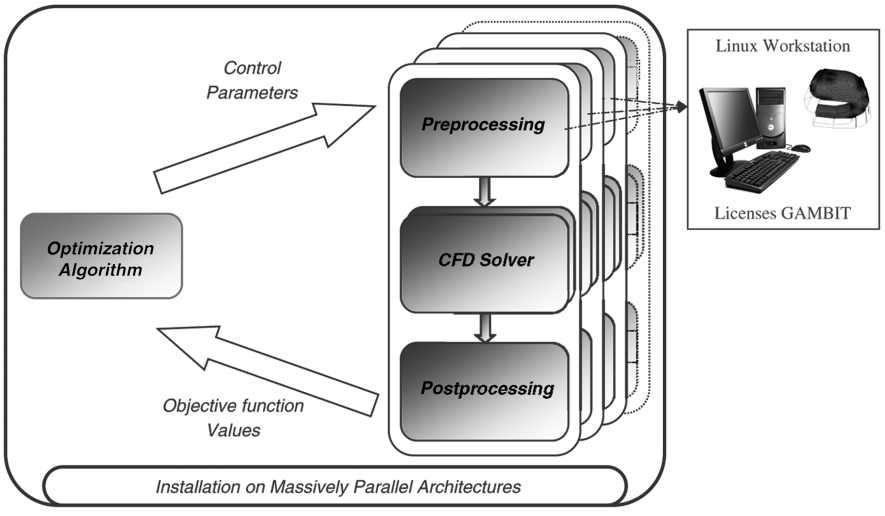

Fig. 1 Schematic representation of the optimization environment tool design with PALM.

3) Detect the conflicts between cost functions by identifying Pareto fronts [52].

The core of the procedure is based on the construction of an approximate model or metamodel [23] (MM) for each objective function. The principal advantage of such MMs is to limit the number of computations involving full 3-D CFD evaluations that are known to be very computer-intensive and time-consuming. The sample databases (DBs) used to compute the MMs are initially constructed from a finite set of CFD runs chosen by a Latin hypercube sampling (LHS) algorithm [53]. The DBs are then iteratively enhanced by adding new samples evaluated by new CFD computations. These evaluations are chosen by parametric operators that give more or less importance to exploration and exploitation. These new samples are chosen based on the uncertainty information contained in the MMs and aim at reducing the uncertainty of the next MMs.

A. Kriging Estimators as Metamodels

In the context of optimization, a wide variety of surrogate models are used in the literature to approximate expensive evaluations of fitness functions. The most prominent methods among all approaches are polynomial models [54], artificial neural networks [55], radial basis function networks [56] and Gaussian processes (GPs) [57]. Among these empirical models, GPs appear to be the most promising for fitness function approximations. Indeed, GPs combine the following decisive properties and were successively applied for combustion problems [24,58]:

1) The implementation of GPs is independent of the number of decision variables.

2) GPs can accurately approximate arbitrary functions including multimodalities and discontinuities.

3) GPs contain meaningful hyperparameters (HPs) that can be obtained theoretically with an optimization procedure.

4) GPs yield an uncertainty measure of the predicted value in the form of a standard deviation.

Two MMs are available in the developed tool. The first one draws inspiration from ordinary kriging [59]. The second one aims at enhancing the behavior of the estimator when faced with noisy functions or badly sampled DBs [60]. Both MMs learn their specific HPs according to the current DBs and yield an estimator $\hat{f}(X)$ of the true function $f(X)$ as well as the standard deviation $\hat{\sigma}_f(X)$ of the predictor for the design point X.

B. Metamodels' Enhancement Operators

For each iteration of the method, the enhancement of the DBs are based on two operators:

1) For each objective i, a search of local optima is performed for the merit function f_M^i defined by

$$f_M^i(X) = \hat{f}_i(X) + \varrho\hat{\sigma}_{f_i}(X) \tag{1}$$

where ϱ is a negative user defined parameter. The value of this parameter controls the conflict between exploration and exploitation. When ϱ tends to 0, the exploitation is fostered. As ϱ decreases, more attention is given to exploration. The local optima are obtained through the use of a multistart strategy [51] of a gradient algorithm [61].

2) The second operator acts in the case of multiobjective studies. It selects the points that belong to the Pareto front, obtained from the MMs with the genetic algorithm *NSGA-II* [62,63], and which have the highest values of $\hat{\sigma}_{f_i}(X)$. The operator then aims at improving the precision of the predicted Pareto front.

The two enhancement operators propose a set of new sample points to be evaluated using the CFD solver. To optimize the use of computational resources (if the number of new samples is not proportional to the number of simultaneous evaluations), a third party can add other samples based on crossover genetic-type operations [64]. It is important to underline that for certain sets of control parameters, the CFD solver may not find acceptable solutions. For these points and to avoid penalization of the merit function, the value of $\hat{\sigma}_{f_i}(X)$ at these locations is suppressed if no information about the objective function is provided (failed CFD) [65,66].

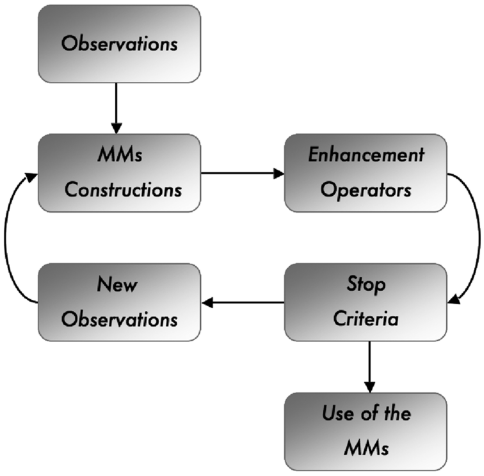

Fig. 2 Flowchart of the proposed strategy to construct the database used to generate the MMs.

The global algorithm is presented in Fig. 2. The initial DBs (depicted by the label "Observations" in the figure) is obtained by a DOE method. Optimal (in the sense of orthogonality and dispersion [67,68]) LHS is generally used for this initialization phase. The stopping criteria for that sequence are the total number of CFD evaluations, the number of new samples obtained by the operators or the overall precision of the MMs. The two steps referred to as "Observations and New Observations" in Fig. 2 consist of evaluating independent sets of design parameters. Consequently and depending on the available computing resources, the different evaluations can be done simultaneously. This feature aims at reducing the overall response time of the method while benefiting from HPC.

IV. Algorithm Verification and Application to a Real Combustion Chamber

A. Methodology Verification and Assessment

To verify the behavior of the implemented optimization method, a simple analytical cost function for a single optimization parameter is considered. For this test and to mimic nonconverged or failed CFD computations, the design space contains a nondefinition zone (NDZ) in which the evaluation of the control parameter is not possible [Eq. (2)]:

$$\begin{aligned} f(X) = f(x) = &-0.01(200 - (x^2 + 5.5x - 11)^2 - (x^2 + x - 7)^2) \\ &- [2.5\exp(-(x-1.5)^2) + 1.3\exp(-(x+4)^2)] \\ &\text{with} \quad x \in [-5, -0.5] \cup [1, 5] \end{aligned} \tag{2}$$

The convergence criterion for which the estimator is considered to be a good representation of the target response function is set to be the L_2 norm of the difference between the analytical target and its estimate. Convergence is in this case set to be below 1% and is kept as such for all of the tests presented in this section. The convergence history of the algorithm is presented in Fig. 3 after the initialization and for the 5 subsequent iterations corresponding to the enrichment of the DBs. With the chosen input parameter, $\varrho = -10$, the merit function converges to the estimator in only 4 iterations. The treatment of the NDZ does not disturb the method which yields final DBs composed of samples that cover the decision space with more concentrations at local and global optima.

As already mentioned, the choice of ϱ has a great impact on the results provided by the method. To more precisely analyze this impact, we consider the analytical multimodal objective function presented in Fig. 4 and given in Eq. (3):

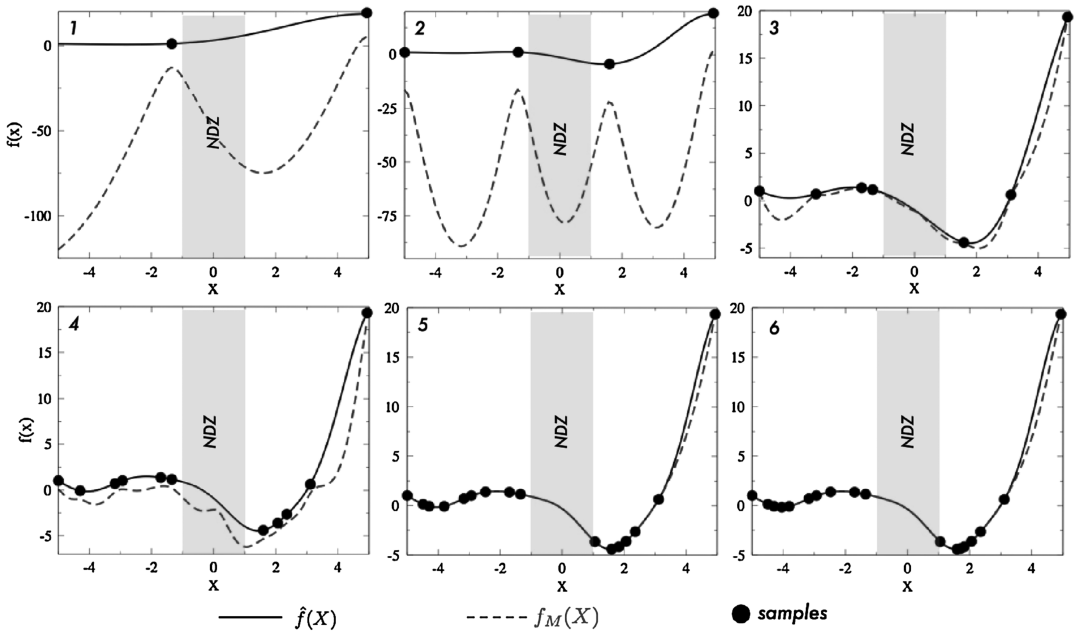

Fig. 3 Verification of the metamodel generation for an analytical case with a NDZ. Successive iterations of the database enrichment: evolution of the merit function, $f_M(X)$, and the metamodel, $\hat{f}(X)$, at the successive iterates.

$$f(X) = f(x,y) = -0.1(x+4)^2 - 3(1-x)^2\exp(-x^2-(y+1)^2) + \exp\left(\frac{-(x+1)^2-y^2}{3}\right) + 10\left(\frac{x}{5}-x^3-y^5\right)\exp(-x^2-y^2)$$
$$\text{with} \quad X \in [-2,2]\times[-2.5,2.5] \tag{3}$$

The experiment aims at observing the convergence rate toward the global optimum (denoted by $X^\star$ in Fig. 4) along with the evolution of the spatial homogeneity of the samples probed in the design space. The last quantity is evidenced by Φ_β [68]:

$$\Phi_\beta(\mathrm{DB}) = \left[\sum_{X^i\in\mathrm{DB}}\sum_{X^j\in\mathrm{DB}X^j\neq X^i} d(X^i,X^j)^{-\beta}\right]^{1/\beta} \tag{4}$$

where $d(X^i, X^j)$ is a measure of the distance separating the points X^i and X^j over the design space.

The precision of the MM which represents the analytical function is also gauged through the parameter rmse (root-mean-square error [69]) evaluated with an external test database DB^T composed of 50 samples:

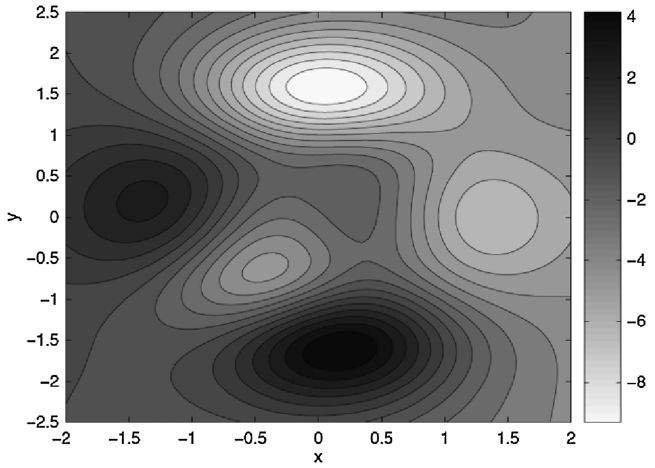

Fig. 4 Two-dimensional multimodal analytical function to be estimated by the MM and for which the convergence impact of the MM parameterization is investigated. The coordinates of the global optimum are $X^\star = (0.0532, 1.5912)$.

$$\mathrm{rsme} = \left[\frac{1}{\mathrm{size}(\mathrm{DB}^T)}\sum_{X\in\mathrm{DB}^T}(\hat{f}(X)-f(X))^2\right]^{1/2} \tag{5}$$

The accuracy of the response surface provided by the MM is assessed in Fig. 5a at each iteration and by comparing $X_{\min}$, the set of optimization parameters that lead to the minimum objective-function value from the current DBs, with $X^\star$. The behavior shows convergence of the method to the global optimum $X^\star$ in the design space and in the objective-function space (Fig. 5b). Clearly, small $|\varrho|$ values yield faster convergence of the method toward $X^\star$ (emphasis on the exploitation concept). The drawback of a fast convergence to $X^\star$ is illustrated in Fig. 6. For small values of $|\varrho|$, the linear increase of Φ_β goes along with a size increase of the current DBs and a homogeneous enhancement of the DBs in the design space. As expected, large values of $|\varrho|$ lead to a homogeneous exploration of the research space. In contrast, small values tend to a fast decrease of the exploration performances. The case $\varrho = -4$ shows the typical behavior of the method: at the early stage of the enhancement, $\hat{\sigma}_{f_i}(X)$ is rather large when compared with $\hat{f}_i(X)$. It produces a homogeneous sampling of the search space. At latter stages, $\hat{\sigma}_{f_i}(X)$ decreases (the predictor becomes better throughout the design space) and the merit function converges to the predictor. The enhancement essentially focuses on new samples located around local optima that degrade the overall homogeneity of the sample distribution (drastic increase of Φ_β).

Based on the previous set of tests, homogeneity in the search space has a direct consequence on the precision of the MM in the design space: if there are too many samples in a reduced region of the design space, the rmse quality measure is degraded (rmse tends to 1). For multiobjective optimization processes, homogeneity is preferred and ϱ is set to a fixed value equal to -10 in the following example.

B. Application to a Real Combustion Chamber

1. *Description of the Target Configuration*

In this section, an application of MIPTO is presented for a Turbomeca combustion chamber (Fig. 7). The supplied CFD computational domain corresponds to one single sector of the fully annular flame tube. Details about the boundary conditions (location and type) as initially supplied are presented in Fig. 8a. The meshes used for this application are unstructured and contain a mean of 210,000 nodes and 1,130,000 tetrahedral cells. The planes used to analyze the CFD predictions as well as illustrations of the turbulent reacting flow within the chamber are presented in Fig. 8b. Note that

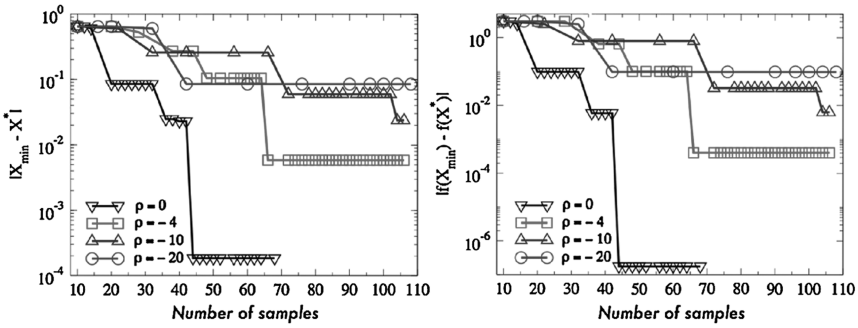

Fig. 5 Illustration of the convergence history for different MM parameters: estimation error for the minimum localization in the parameter space (left) and absolute error in the function space (right).

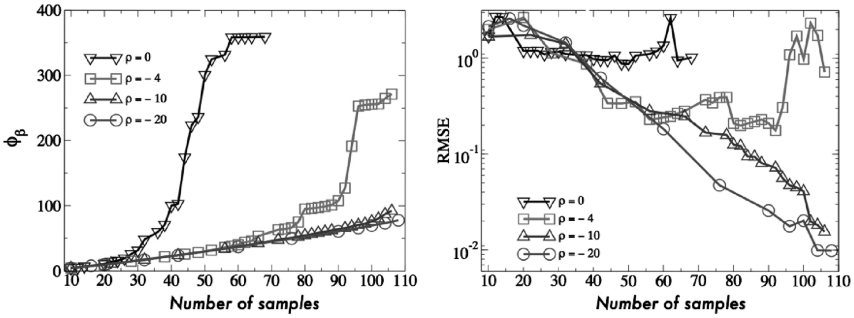

Fig. 6 Impact of the different parameters on the search space sample distribution: estimation of the space sample density (left) and its rmse (right).

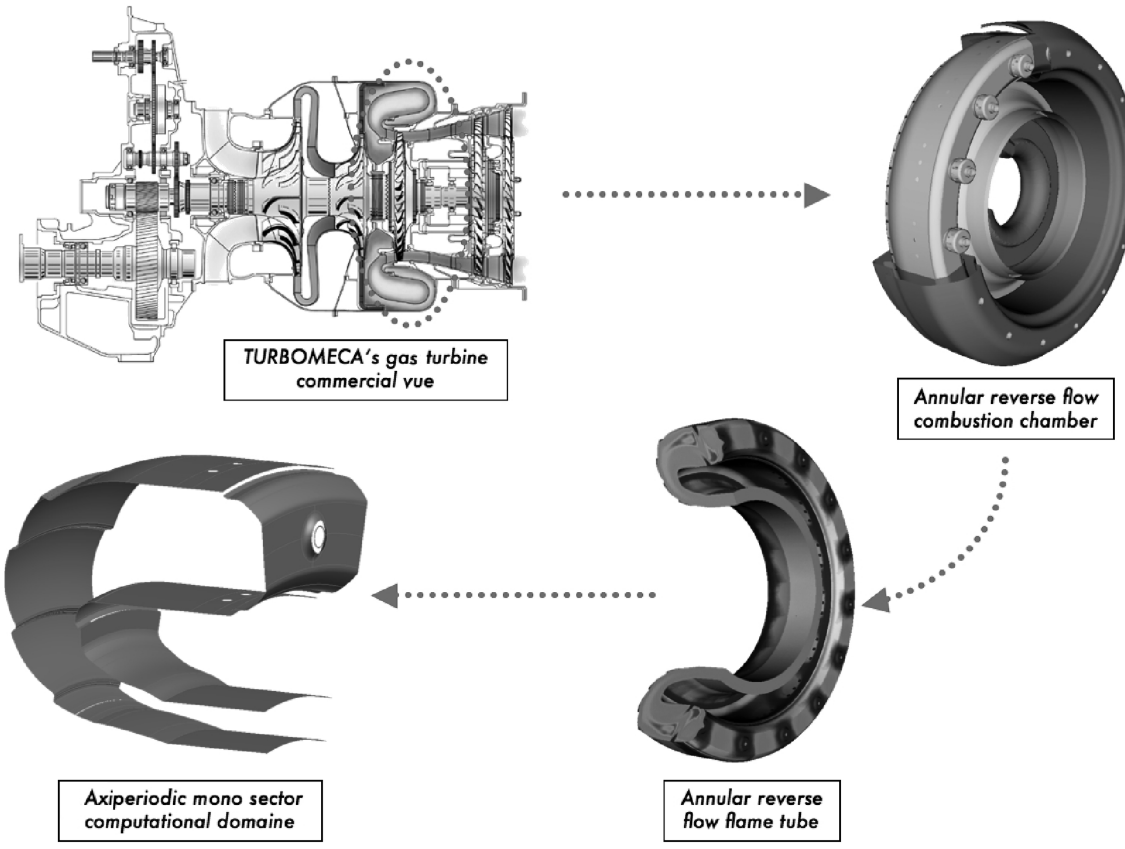

Fig. 7 Industrial configuration targeted for the optimization.

plane 4 coincides here with the location of the distributor, which is a critical element of the engine. Indeed, the distributor is subject to large thermal stresses due to the temporal and azimuthal temperature variations induced by combustion taking place in the primary zone of the combustion chamber (region delimited by the primary jets as well as the swirled injector). One aim of the current application is to reduce that thermal stress, hence improving the design of the given chamber for a given operating point.

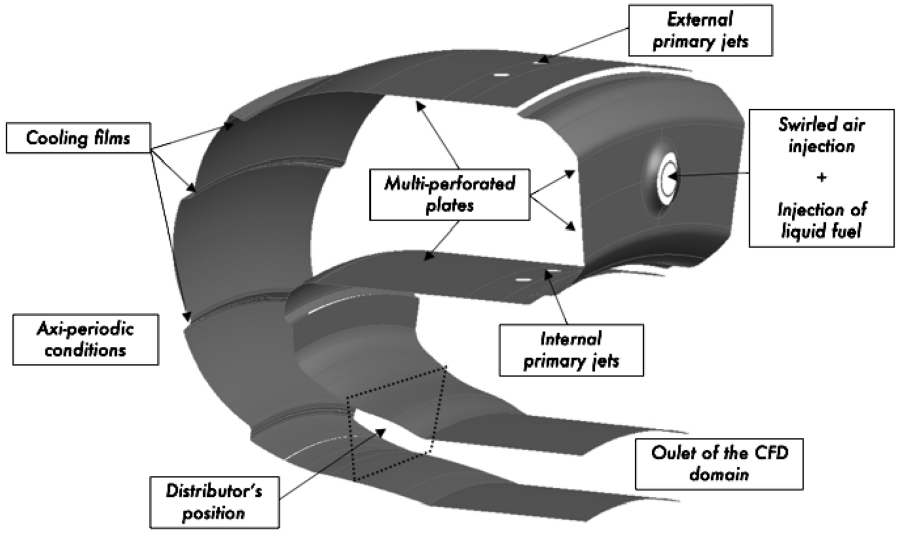

a)

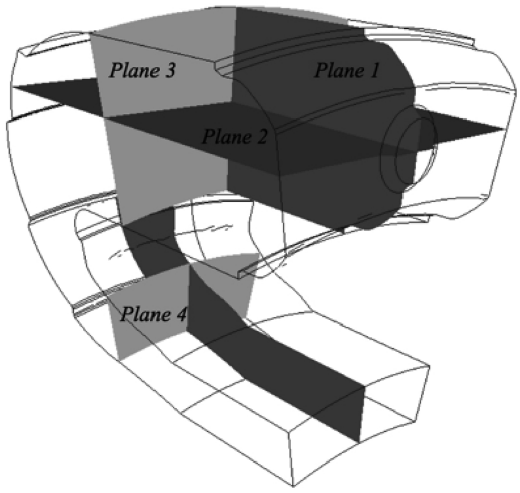

b)

Fig. 8 CFD initial model retained for the analysis by the optimization algorithm: a) CFD computational model and its boundary conditions and b) planes used for the CFD diagnostics and analyses.

2. Presentation of the Baseline Configuration

Figure 9 presents the dimensionless aerodynamic and combustion fields of the reference design. Most of the aerodynamic activity concentrates in the primary zone of the combustion chamber. In this region, a large recirculation zone located after the air injector characterizes the flow. The external primary jets bring air within the primary zone to ease combustion. The effect of the internal jets on that part of the chamber is not so clear. Flow streamlines in plane 1 of the chamber show an important recirculation zone located after the external primary jets. Note that the recirculating gases of the primary zone lead to fast evaporation and mixing of the liquid fuel injected through the swirler. Combustion, visualized through the reaction rate (Fig. 9d), takes place in the vicinity of the swirler. Fuel that is not burned in the primary zone is consumed near air-admission orifices, mostly in the neighborhood of the external primary jets. Finally, temperature maps (nondimensionalized by the fresh air temperature T_3) in plane 1 (Fig. 9e) and plane 2 (Fig. 10a) underline the trajectories of hot gases when leaving the primary zones.

3. Definition of the Optimization Problem

The considered optimization process deals with two conflicting objectives. The first one consists of maximizing the combustion efficiency η_c. Following Lefebvre [70], combustion efficiency for the studied system can be expressed in terms of a parameter denoted by θ and defined by

$$\eta_c = f(\theta) = f\left(\frac{P_3^n V_c \exp(T_3/T_{\text{ref}})}{\dot{m}_a}\right) \tag{6}$$

where P_3 and T_3 are the pressure and the temperature of the air supplied by the compressor, $\dot{m}_a$ is the air mass flow entering the primary zone of the flame tube, and V_c is its volume. The maximization of V_c (or the minimization of the inverse of θ) leads to a maximization of the combustion efficiency.

The second objective deals with the thermal stress imposed by the hot gases impacting the distributor (Fig. 11). A relevant measure of this stress is the profile factor at the stator location [70] Pr_f^s, given by

$$Pr_f^s = \frac{\max(T_4(r)) - T_4}{T_4 - T_3} \tag{7}$$

where T_4 is the mean exit chamber temperature, and $\max(T_4(r))$ is the maximum value of the exit radial temperature, illustrated in Fig. 11. Note that minimizing the profile factor increases life expectancy of the stator and the engine.

The control parameters used to minimize the objective functions (Pr_f^s, θ^{-1}) are of two kinds:

1) With the geometric parameter, the relative distance from the swirler location to the external and internal jets is noted as P_{pi}. Note that the axial distance that separates the external and internal jets is kept constant.

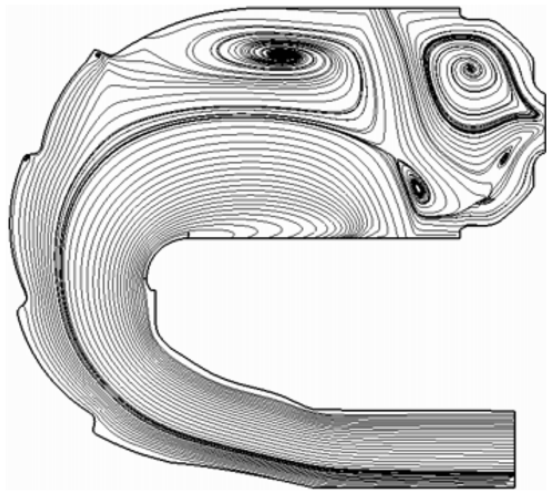

a)

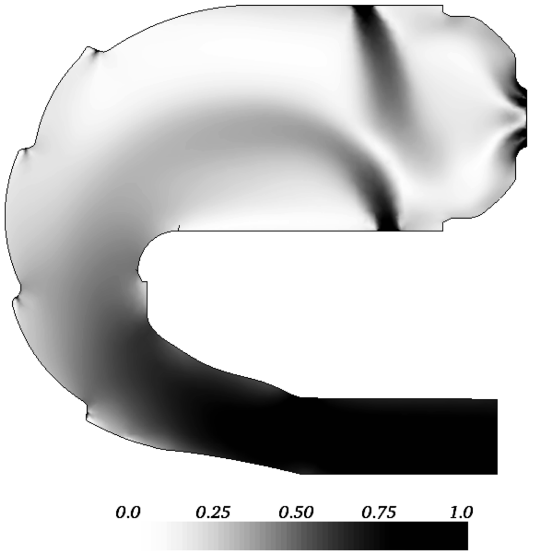

b)

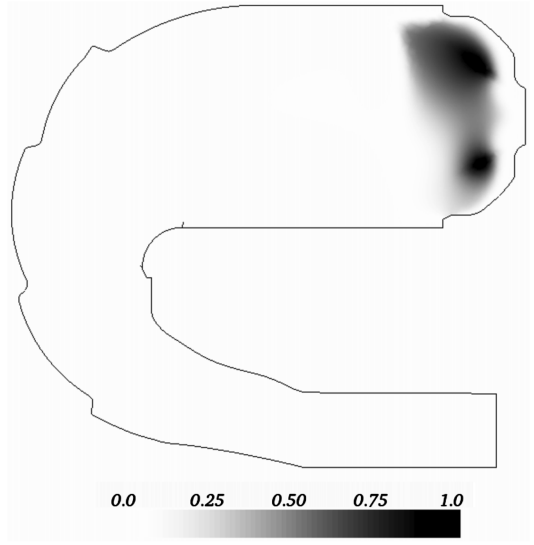

c)

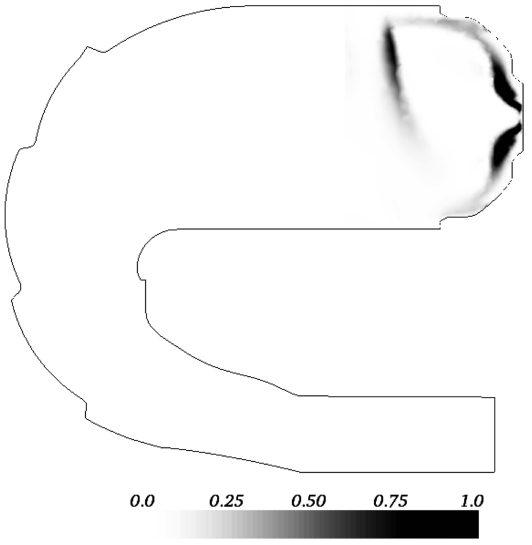

d)

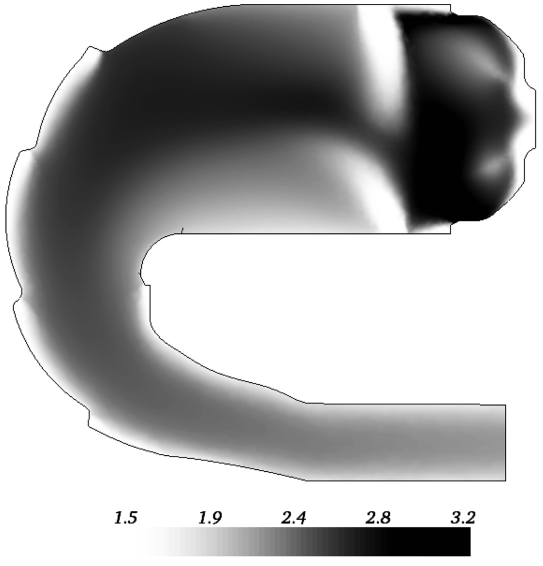

e)

Fig. 9 Reference configuration flowfield as obtained with CFD in plane 1 (cf. Fig. 8b): a) velocity streamlines, b) velocity magnitude, c) fuel/air ratio, d) reaction rate, and e) temperature map divided by T_3.

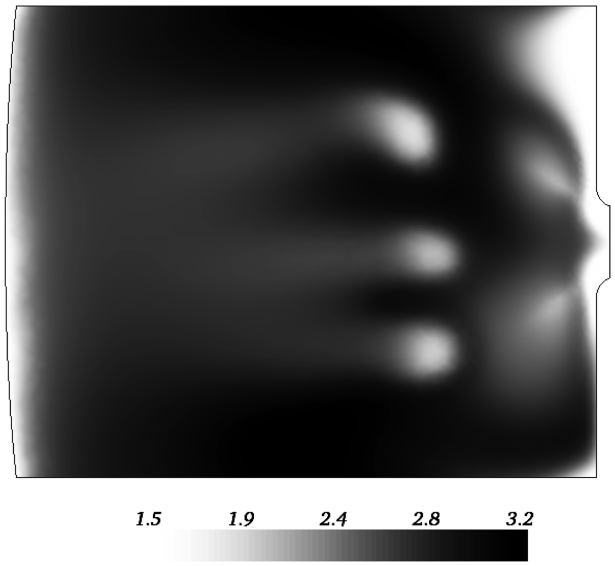

a)

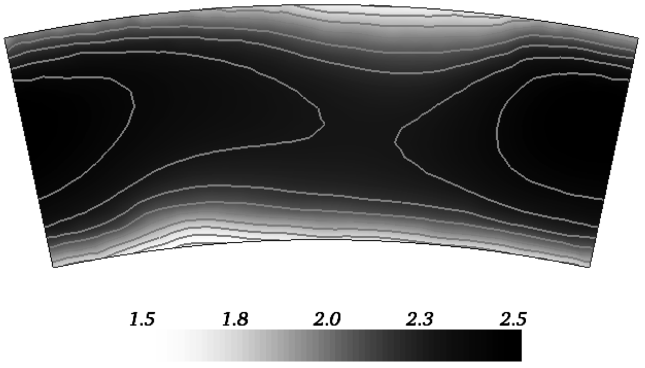

b)

Fig. 10 Reference configuration: temperature field divided by T_3 as obtained by CFD: a) in plane 2 and b) at the exit plane of the combustion chamber.

2) With the flow-conditions parameter, the total air mass flow is kept constant. Only the airflow split between the internal and external multiperforated plates and the swirler are changed (i.e., P_{mp} and P_{dt}, respectively).

Figure 12 illustrates the optimization parameters. In the following, the superscript b corresponds to the baseline configuration. To keep a constant total air mass flow rate entering the flame tube, which ensures the reference operating point, constraints need to be defined on the optimization problem. For our test, the total amount of air flowing through the multiperforated plates, Q_{MP}, and through the swirler, Q_T, are adjusted to satisfy

$$Q_T = Q_T^b P_{dt} \tag{8}$$

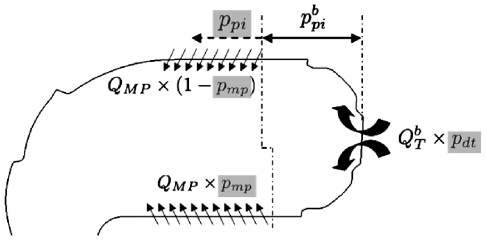

Fig. 12 Description of the optimization parameters and the constraints used for the optimization process of the engine.

$$Q_{\mathrm{MP}} = Q_{\mathrm{MP}}^b + Q_T^b(1 - P_{dt}) \tag{9}$$

$$Q_{\mathrm{MP}}^i = P_{mp}((1 - P_{dt})Q_T^b + Q_{\mathrm{MP}}^b) \tag{10}$$

$$Q_{\mathrm{MP}}^e = (1 - P_{mp})((1 - P_{dt})Q_T^b + Q_{\mathrm{MP}}^b) \tag{11}$$

Variations at the swirler inflow are imposed using scale similarity (proportionality) on the velocity profiles specified at the swirler inlet boundary condition of the CFD run. Similarly, multiperforated inflow conditions necessitate the specification of a velocity V proportional to the plate's porosity σ, its surface area S, and the local flow density ρ:

$$Q = \rho S V \sigma \tag{12}$$

$$\sigma^i = \frac{Q_{\mathrm{MP}}^i(P_{dt}, P_{pi})}{S^i(P_{pi})} \times \left(\frac{S^i\sigma^i}{Q^i P_{\mathrm{MP}}^i}\right)^b \tag{13}$$

$$\sigma^e = \frac{Q_{\mathrm{MP}}^e(P_{dt}, P_{pi})}{S^e(P_{pi})} \times \left(\frac{S^e\sigma^e}{Q^e P_{\mathrm{MP}}^e}\right)^b \tag{14}$$

In the preceding expressions, the superscripts i and e, respectively, denote the internal and external surfaces. The quantity in parenthesis with the b superscript refers to a ratio evaluated for the original design.

The optimization problem then looks for the optimal choices of

$$\min \begin{cases} Pr_f^s \\ \theta_{\mathrm{f}}^{-1} \end{cases} \quad \text{with} \quad \begin{cases} P_{pi} \in [0, P_{pi}^{\max}], \\ P_{dt} \in [P_{dt}^{\min}, 1], \\ P_{mp} \in [P_{mp}^{\min}, P_{mp}^{\max}] \end{cases} \tag{15}$$

4. *Results of the Optimization Process*

For the problem considered, one CFD evaluation for a given set of control parameters requires approximately 168 CPU hours, which corresponds to 6 wall-clock hours or elapsed time if using 28 processors of a IBM JS1 Power5 1.5 GHz processor. The

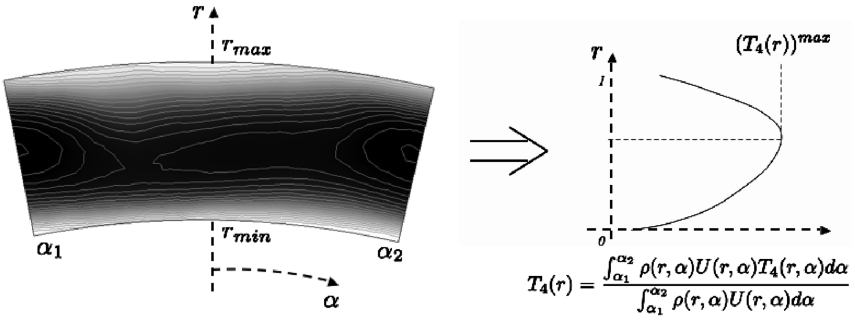

Fig. 11 Information extracted from the CFD run and quantity analyzed by the optimization process.

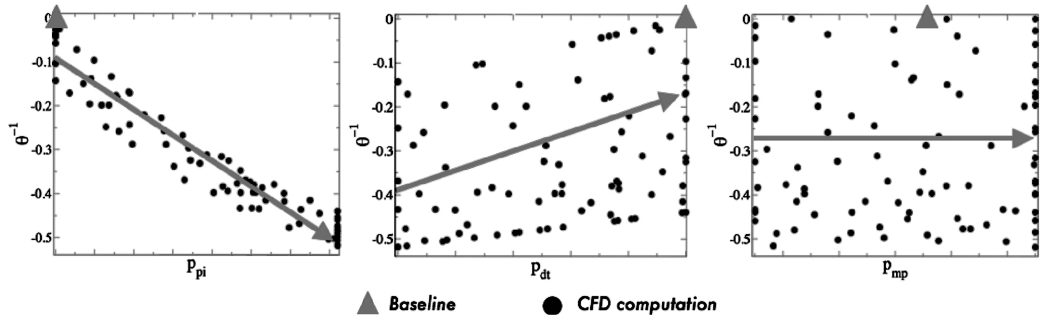

Fig. 13 Scatter plots of the combustion efficiency as a function of the other parameters and obtained by CFD at the requested points in the search space.

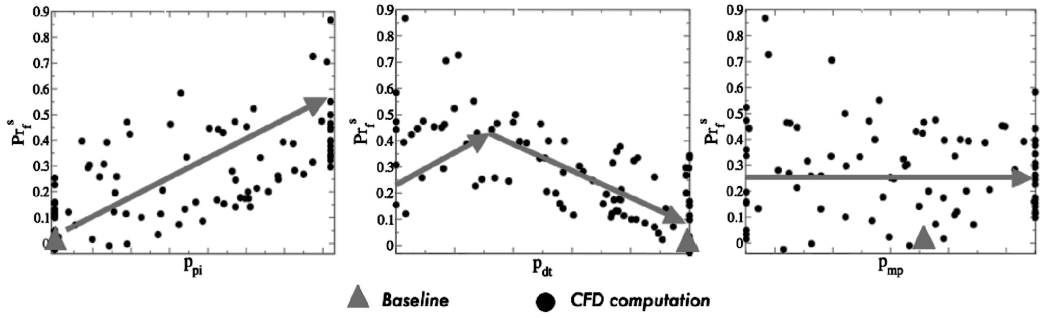

Fig. 14 Scatter plots of the exit-temperature profile factor as a function of the other parameters and obtained by CFD at the requested points in the search space.

enhancement of the DBs is limited to 100 CFD computations (714 CPU days on 28 processors is 25.5 days) and the initialization of the DBs is set to provide 30 samples (210 CPU days on 28 processors is 7.5 days). From the 100 CFD runs, the algorithm discards 14% of the predictions (unphysical results) to construct the MMs. For confidentiality reasons, the presentation of the results uses dimensionless quantities:

$$(Pr_f^s(P))^a = \frac{Pr_f^s(P) - (Pr_f^s)^b}{(Pr_f^s)^b} \tag{16}$$

$$(\theta^{-1}(P))^a = \frac{\theta^{-1}(P) - (\theta^{-1})^b}{(\theta^{-1})^b} \tag{17}$$

This normalization is to be interpreted with respect to the performance of the reference design: negative values correspond to improved criteria and positive values indicate degradation. Note also that both objective functions depend on $P = (P_{mp}, P_{dt}, P_{pi})$.

The analysis of the data provided by the enhancement process is presented in two steps. The first step, inspired from sensitivity analyses [71], aims at better understanding relationships between control parameters and objective functions. The second step deals with the actual search for interesting new configurations after going through the optimization process.

When the number of control parameters or objective functions is quite large, sensitivity measures [72,73] can guide the designer in distinguishing which parameters are the most important. For our application, one can directly analyze the objective-function responses through scatter plots (Figs. 13 and 14). The combustion-efficiency parameter θ^{-1} is mostly dependent on the position of primary jets P_{pi} and, to a lesser extent, on the airflow split parameter P_{dt}. These behaviors are explained in light of the mathematical expression of θ^{-1}, where V_c depends on P_{pi} and $\dot{m}_a$ depends on P_{dt}:

$$\theta^{-1} = \frac{\dot{m}_a(P_{dt})}{P_3^n V_c(P_{pi}) \exp(T_3/T_{\text{ref}})} \tag{18}$$

The objective Pr_f^s depends on P_{pi} and P_{dt}. The role played by the mass flow passing through the external and internal multiperforated plates to feed the dilution process is not detectable by Pr_f^s. The dependency of Pr_f^s along the design space is not as trivial as for θ^{-1}. Focusing on the P_{pi} parameter, moving the primary jets downstream leads to an increased volume of the primary zone, which contributes to a more complete combustion. The major drawback is a shortened dilution length and poorer mixing of the hot products by fresh gases. Hence, the Pr_f^s criterion is degraded. Looking at the effect of P_{dt}, one notes that below a critical value, the excess of fuel in the primary zone is consumed by the air provided by the primary jets. Mixing and dilution of hot gases by these jets is no longer efficient, and the small amount of cold air to be injected by the multiperforated plates is insufficient. Once again, the Pr_f^s criterion is degraded. Beyond the critical value of P_{dt}, combustion in the primary zone is increasingly complete and the primary jets play their intended role by properly mixing the hot gases (i.e., Pr_f^s is improved).

Figure 15 presents the results of the optimization in the objective-function space. The feasible domain and the Pareto front have been determined from the MMs constructed from DBs containing 88 CFD evaluations. Based on the position of the feasible domain in the objective-function space, the optimization process allows for

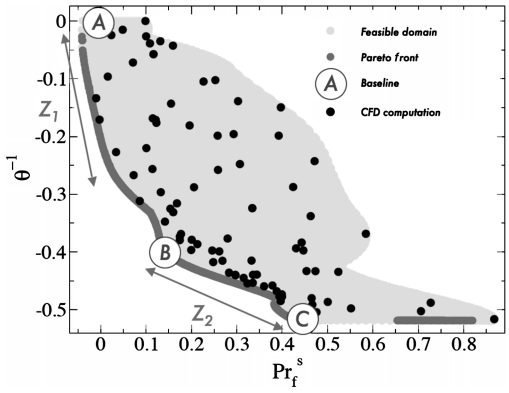

Fig. 15 Pareto front as identified for the multiobjective optimization along with reference configuration A and two potential candidates B and C for an improved engine configuration.

Table 1 Coordinates of the designs analyzed in the document

	$\%[P_{dt}^{\min};1]$	$\%[0;P_{pi}^{\max}]$	$\%[P_{pm}^{\min};P_{pm}^{\max}]$	$(Pr_f^s)^a$	$(\theta^{-1})^a$
Reference A	100	0	61	0	0
Candidate B	57	71	100	0.14	−0.39
Candidate C	0	100	100	0.44	−0.52

potential improvement of the combustion efficiency and degradation of the thermal criterion at the distributor location (plane 4). Two separate zones are highlighted on the Pareto front. In the first one, noted as Z_1, it is possible to drastically improve the combustion efficiency without degrading Pr_f^s too much:

$$Z_1\colon \left(\theta^{-1}, Pr_f^s\right) \in [-0.35;0] \times [-0.1;0.1]$$

In contrast, in the second region, noted as Z_2, small improvements of θ^{-1} lead to large degradation of Pr_f^s:

$$Z_2\colon \left(\theta^{-1}, Pr_f^s\right) \in [-0.5;-0.4] \times [0.15;0.45]$$

Figure 15 also underlines the fact that in the second region of the Pareto front, a large density of samples locates near the Pareto front. The method has found new interesting compromises during the last iteration, and the new approximation of the Pareto front has not yet been explored by the enhancement operators. This also highlights the fact that the method has not yet converged to the true Pareto front of the multiobjective problem. However, a compromise between computational time and convergence properties of the results needs to be set for practical applications. Despite the mentioned shortcoming, two new design points detailed in Table 1 seem interesting in the context of the optimization process. These potential new designs are analyzed subsequently (Figs. 16–18). The baseline configuration is presented in Figs. 9 and 10 for comparisons.

The first compromise is located along the Pareto front, between the two identified zones of the response-function space. The second design corresponds to an improved combustion efficiency and a degraded Pr_f^s when compared with the previous point. Figure 16 illustrates the main flow-topology differences between the two designs, Fig. 17 concentrates on the fuel repartition and temperature distributions, and Fig. 18 shows the exit-temperature maps. As underlined and identified in practice when defining a new combustion chamber [70], the flow topology is greatly influenced by the position of the primary and dilution jets. When these jets are moved downstream (away from the swirler), increasingly complex flow structures coexist in the primary zone. A second consequence of

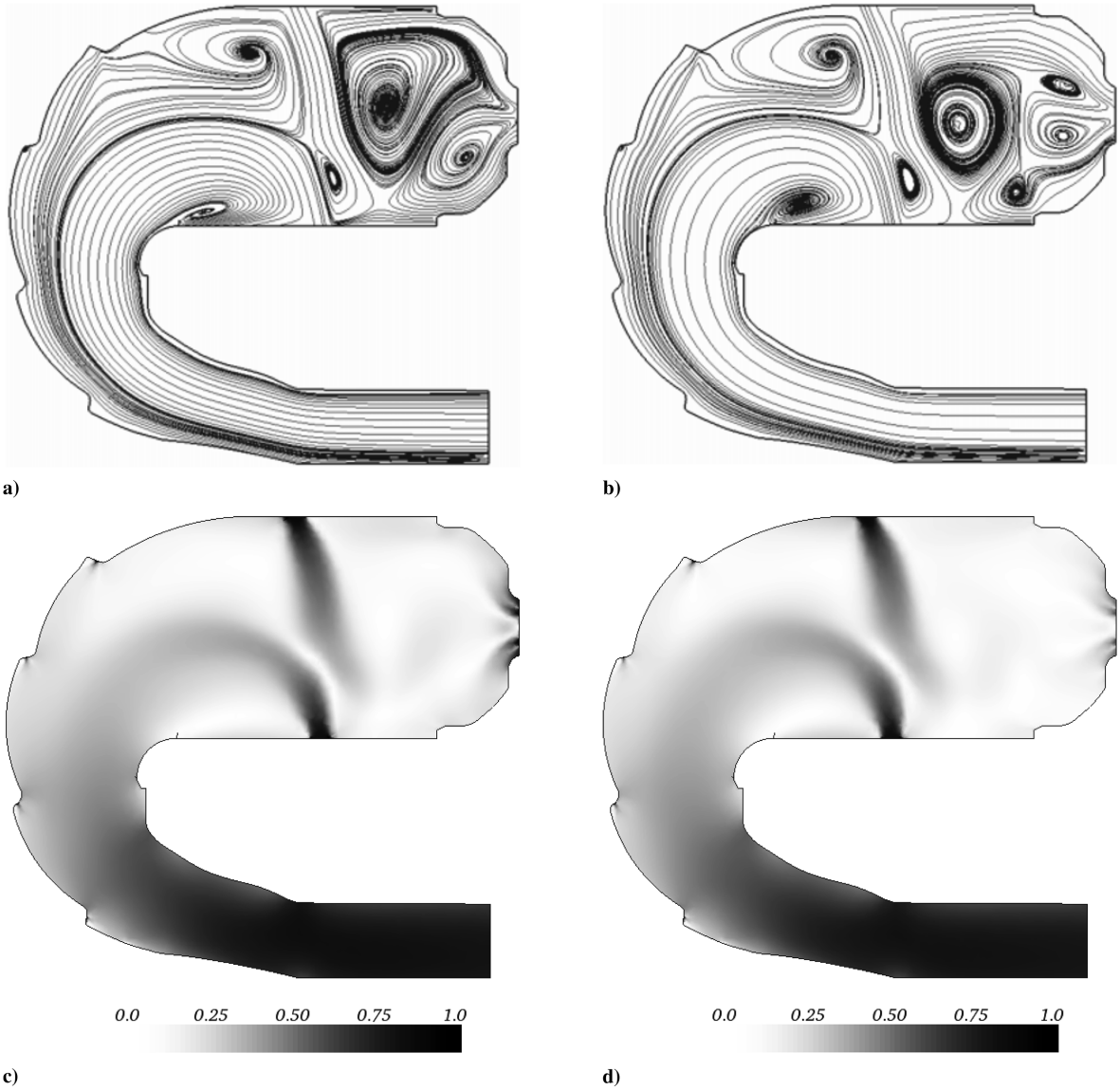

Fig. 16 Flowfield visualization in plane 1 (cf. Fig. 8b) of the aerodynamic quantities obtained by CFD for the two potential candidates for an improved engine configuration of point B (left) and point C (right), as defined in Fig. 15: a–b) velocity streamlines and c–d) velocity magnitude. For comparisons with reference configuration A, see Fig. 9.

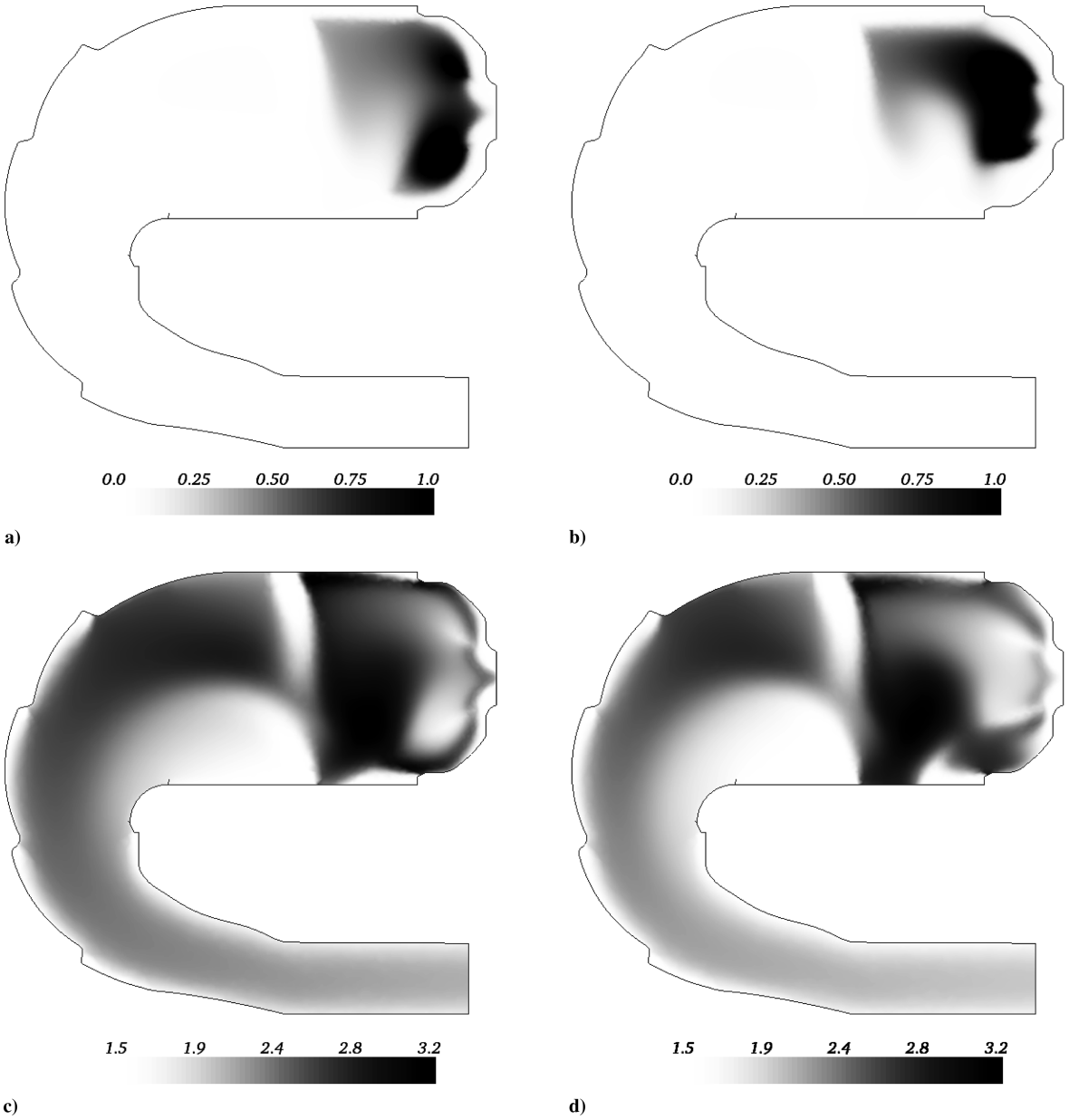

Fig. 17 Flowfield visualization in plane 1 (cf. Fig. 8b) of the combustion quantities obtained by CFD for the two potential candidates for an improved engine configuration of point B (left) and point C (right), as defined in Fig. 15: a–b) fuel/air ratio and c–d) temperature divided by T_3. For comparisons with reference configuration A, see Fig. 9.

the primary jet adjustment is the reduction in intensity of the recirculation zone positioned behind the external jets, which is responsible for a large part of the mixing of the hot products with fresh gases. The reduction in size of that flow structure goes along with the intensification of a second recirculation zone positioned behind the internal jets and has a limited impact on mixing. Finally, and as expected with the changes in the primary and dilution zones inferred by the set of parameters, the new designs yield different exit-temperature fields (Fig. 18). For the retained cases, spatial heterogeneity of the exit-temperature fields is clearly observed when compared with the reference case, the original design being the optimum.

Based on the previous set of results, several rules of design can be inferred to efficiently obtain a combustion chamber that is optimal in term of combustion efficiency and exit-temperature profile. Although necessary to shield the chamber walls from the hot product of combustion, the multiperforated plates do not influence the exit-temperature profile. For this specific objective, the leading parameters are the jet position and the flow rate of fresh air that is available for injection at this location. The outer jet also plays a critical role for combustion. If not penetrating the primary zone, fuel is burned in the mixing region of the chamber (outside the primary zone), thereby ruining the exit-temperature profile. Combustion efficiency essentially depends on the primary-zone volume or,

Table 2 Wall-clock time for the optimization of different computational domain of an aeronautical gas turbine engine and as a function of the available computing power

Number of processors	16	32	64	128	256	2048	4096
Single sector flame tube, days	65.6	32.8	16.4	8.2	4.1	0.5	0.25
Single sector flame tube and its casing, days	85.3	42.6	21.3	10.7	5.3	0.7	0.3
Complete annular chamber, days	1280	640	320	160	80	10	5

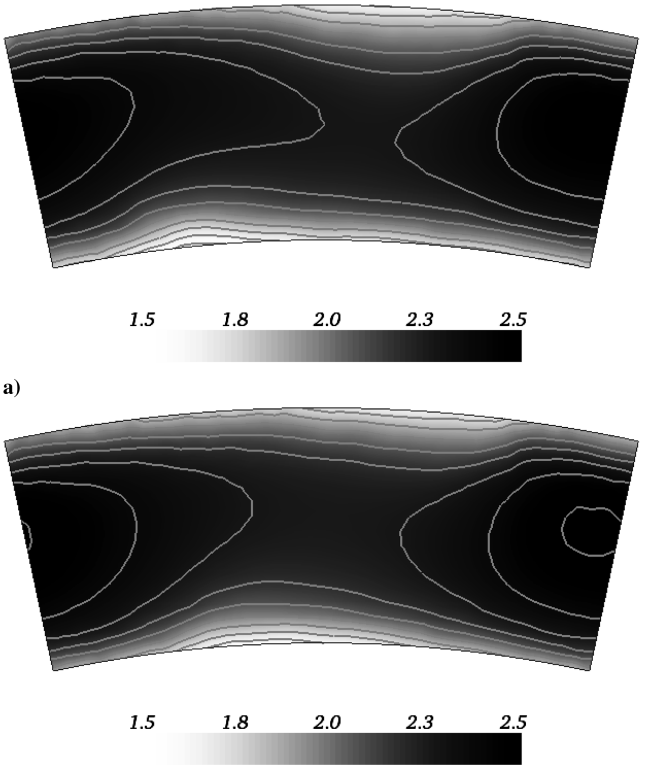

Fig. 18 Temperature fields divided T_3 at the exit of the combustion chamber (plane 4 of Fig. 8b) obtained by CFD for the two potential candidates for an improved engine configuration: a) configuration B and b) configuration C.

equivalently, the outer-jet position. The aim of the designer is thus to have the proper location of the primary jets as well as the airflow split between the swirler and these jets. The design also needs to ensure sufficient outer-jet penetration in the primary zone, which guarantees complete combustion in this region while allowing proper mixing of the hot product before exiting the chamber. All other parameters seem to have second-order effects.

Preliminary conclusions resulting from the application of the optimization tool to full three-dimensional multiphase reacting CFD are as follows:

1) Optimization using MMs along with initial DBs of 30 CFD runs proves to be feasible with available HPC power and within industrial constraints.

2) Although convergence of the estimated cost functions is not fully ensured after 100 CFD evaluations, the tool recovers know-how obtained by experienced engineers on this specific chamber, as follows:

a) Multiperforated plates have a small impact on the profile factor at the stator location and on the combustion efficiency.

b) The primary jet axial position is of foremost importance and increased efficiency usually results in a decreased exit-temperature homogeneity for the configuration investigated.

A recapitulation of the computer costs involved by the use of such an optimization tool is given in Table 2 (note that these numbers are only obtained if the application scales ideally, which is not guaranteed for the CFD solver, for example). Projections are added based on the fact that current CFD codes scale almost linearly, to further emphasize the potential impact of HPC on today's engineering work in the field of gas turbine engines.

V. Conclusions

Massively parallel architectures give access to huge computing power and provide new possibilities for the development of tools to be used for the definition of new designs of industrial products. Among the impacted fields, the design of the aeronautical combustion chambers still relies heavily on engineering know-how and experience. Although turbulent reacting-flow predictions by use of CFD applications is extensively used today by industry for the design of the next generation of combustion chambers, the amount of personnel effort and CPU cost required by these computations prevent extensive design testing or improvements. In fact, and contrary to the realm of aerodynamics, the constraints are so important that optimization strategies using CFD codes are scarce in the context of combustion. In this work, a preliminary demonstration of the feasibility of a fully automated decision-making tool for combustion chambers is provided. The adopted multiobjective optimization strategy relies on turbulent reacting CFD runs and HPC. To limit the impact of many evaluations of flow computations that are CPU- and time-consuming, metamodels are introduced along with a DOE approach. The main contribution of this work lies in the search for optima that are obtained from a metamodel that is automatically improved, based on new CFD computations and quality estimators detailed earlier. Specific issues linked to the management of parallel applications for efficient use of HPC are also addressed. Verifications and sensitivity of the proposed strategy are presented for simple optimization problems based on analytical expressions. To conclude, the application of the new tool to a real gas turbine combustion chamber proves to be feasible with available computing power and yields manageable response time. For an industrial combustion chamber, the aim of the optimization is to improve an existing design in terms of engine durability and efficiency. Two potential new candidates are proposed along with a parameter sensitivity analysis and the identification of the Pareto front. Finally, the tool provides design rules in agreement with the know-how gained by experienced engineers for this type of configuration.

Acknowledgments

The authors gratefully acknowledge the implication of Turbomeca for its support as well as the Centre Informatique National de l'Enseignement Supérieur (CINES) located in Montpellier, France, for computer access to its facility. Financial support for this research activity is provided by the European project Intellect DM (Integrated Lean Low-Emission Combustor Design Methodology) coordinated by Rolls-Royce Deutschland.

References

[1] Cusdin, P., and Müller, J., "Generating Efficient Code with Automatic Differentiation," *ECCOMAS 2004*, Univ. of Jyväskylä, Jyväskylä, Finland, 2004, http://www.mit.jyu.fi/eccomas2004/proceedings/pdf/1115.pdf.

[2] Anderson, W., and Nielsen, E., "Aerodynamic Design Optimization on Unstructured Grids with a Continuous Adjoint Formulation," *Computers and Fluids*, Vol. 28, No. 4, 1999, pp. 443–480. doi:10.1016/S0045-7930(98)00041-3

[3] Césaré, N. D., "Outils pour l'Optimisation de Forme et le Contrôle Optimal, Application à la Mécanique des Fluides," Ph.D. Thesis, Univ. de Paris 6, Paris, 2000.

[4] Jameson, A., Sriram, Matinelli, L., and Haimes, B., "Aerodynamic Shape Optimization of Complete Aircraft Configurations Using Unstructured Grids," 42nd AIAA Aerospace Science Meeting and Exhibit, AIAA Paper 2004-0533, Jan. 2004.

[5] Mohammadi, B., "Optimization of Aerodynamic and Acoustic Performances of Supersonic Civil Transports," *Proceedings of the Summer Program*, Center for Turbulence Research, Stanford Univ., Stanford, CA, 2002, pp. 285–296.

[6] Martins, J., "A Coupled-Adjoint Method for High-Fidelity Aero-Structural Optimization," Ph.D. Thesis, Stanford Univ., Stanford, CA, 2002.

[7] Leoviriyakit, K., "Wing Planform Optimization Via An Adjoint Method," Ph.D. Thesis, Stanford Univ., Stanford, CA, 2005.

[8] Duvigneau, R., "Contribution à l'Optimisation de Forme pour des Ecoulements à Fort Nombre de Reynolds Autour de Géométries Complexes," Ph.D. Thesis, Ecole Centrale de Nantes, Nantes, France, 2002.

[9] Lewis, R., Torczon, V., and Trosset, M., "Why Pattern Search Works," *Optimal Control Applications and Methods*, Vol. 59, Oct. 1998, pp. 1–7.

[10] Hooke, R., and Jeeves, T., "Direct Search Solution of Numerical and Statistical Problems," *Journal of the Association for Computing Machinery*, Vol. 8, No. 2, 1961, pp. 212–229. doi:10.1145/321062.321069

[11] Abramson, D., and Peachey, A. L. T., and Flecher, C., "An Automatic Design Optimization Tool and Its Application to Computational Fluid Dynamics," *Conference on High Performance Networking and Computing: Proceedings of the 2001 ACM/IEEE conference on Supercomputing* [CD-ROM], Vol. 10, Association for Computing Machinery, New York, 2001. doi:10.1145/582034.582059

[12] Lewis, A., Abramson, D., and Peachey, T., "RSCS: A Parallel Simplex Algorithm for the Nimrod/O Optimization Toolset," *ISPDC 2004: Third International Symposium on Parallel and Distributed Computing*, IEEE Computer Society, Washington, D.C., 2004, pp. 71–78.

[13] Eldred, M., Giunta, A., Wa, B. V. B., Wojtkiewicz, S., Hart, W., and Alleva, M., "DAKOTA, A Multilevel Parallel Object-Oriented Framework for Design Optimization, Parameter Estimation, Uncertainty Quantification, and Sensitivity Analysis," Sandia National Labs., Rept. SAND2001-3514, Albuquerque, NM, 2002.

[14] Berghen, F., "CONDOR: A Constrained, Non-Linear, Derivative-Free Parallel Optimizer for Continuous, High Computing Load, Noisy Objective Functions," Ph.D. Thesis, Univ. Libre de Bruxelles, Brussels, 2004.

[15] Meza, J., Oliva, R., Hough, P., and Williams, P., "OPT + + An Object-Oriented Toolkit for Nonlinear Optimization," *ACM Transactions on Mathematical Software*, Vol. 33, No. 2, 2007, p. 12. doi:10.1145/1236463.1236467

[16] Pätzold, M., Lutz, T., Krämer, E., and Wagner, S., "Numerical Optimization of Finite Shock Control Bumps," 44th AIAA Aerospace Science Meeting and Exhibit, AIAA Paper 2006-1054, Jan. 2006.

[17] Ricci, S., and Terraneo, M., "Conceptual Design of an Adaptive Wing for a Three-Surfaces Airplane," 46th AIAA/ASME/ASCE/AHS/ASC Structures, Structural Dynamics, and Materials Conference, AIAA Paper 2005-1959, Austin, TX, Apr. 2005, pp. 1–14.

[18] Luersen, M., Riche, R. L., Lemosse, D., and Maître, O. L., "A Computationally Efficient Approach to Swimming Monofin Optimization," *Structural and Multidisciplinary Optimization*, Vol. 31, No. 6, Apr. 2006, pp. 488–496. doi:10.1007/s00158-006-0001-6

[19] Nelson, A., Nemec, M., Aftosmis, M., and Pulliam, T., "Aerodynamic Optimization of Rocket Control Surfaces Using Cartesian Methods and CAD Geometry," 23rd AIAA Applied Aerodynamics Conference, AIAA Paper 2005-4836, Toronto, June 2005.

[20] Kelner, V., Grondin, G., Ferrand, P., and Moreau, S., "Robust Design and Parametric Performance Study of an Automotive Fan Blade by Coupling Multi-Objective Optimization and Flow Parameterization," *Proceedings of the International Congress on Fluid Dynamics Application in Ground Transportation*, Société des Ingénieurs de l'Automobile, Suresnes, France, Oct. 2005.

[21] Marco, N., Lanteri, S., Désidéri, J., and Périaux, J., "A Parallel Genetic Algorithm for Multi-Objective Optimization in Computational Fluid Dynamics," *Evolutionary Algorithms in Engineering and Computer Science*, edited by K. Miettinen, M. M. Mäkelä, P. Neittaanmäki, and J. Périaux, Wiley, Hoboken, NJ, 1999, pp. 445–456.

[22] Muyl, L., Dumas, F., and Herbert, V., "Hybrid Method for Aerodynamic Shape Optimization in Automotive Industry," *Computers and Fluids*, Vol. 33, Nos. 5–6, 2004, pp. 849–858. doi:10.1016/j.compfluid.2003.06.007

[23] Kleijnen, J., "A Comment on Blanning's Metamodel for Sensitivity Analysis: The Regression Metamodel in Simulation," *Interfaces*, Vol. 5, No. 3, 1975, pp. 21–23.

[24] Jeong, S., Minemura, Y., and Obayashi, S., "Optimization of Combustion Chamber for Diesel Engine Using Kriging Model," *Journal of Fluid Science and Technology*, Vol. 1, No. 2, 2006, pp. 138–146. doi:10.1299/jfst.1.138

[25] Fleming, P., Purshouse, R., and Lygoe, R., "Many-Objective Optimization: An Engineering Design Perspective," *Proceedings of Evolutionary Multi-Criterion Optimization*, Vol. 3410, Springer, New York, 2005, pp. 14–32.

[26] Ray, T., and Tsai, H., "Swarm Algorithm for Single and Multiobjective Airfoil Design Optimization," *AIAA Journal*, Vol. 42, No. 2, 2004, pp. 366–423. doi:10.2514/1.9099

[27] Coehlo, R., "Multicriteria Optimization with Expert Rules for Mechanical Design," Ph.D. Thesis, Univ. Libre de Bruxelle, Brussels, 2004.

[28] Büche, D., "Multi-Objective Evolutionary Optimization of Gas Turbine Components," Ph.D. Thesis, Swiss Federal Inst. of Technology, Zurich, 2003.

[29] Obayashi, S., Tsukahara, T., and Nakamura, T., "Multiobjective Evolutionary Computation for Supersonic Wing-Shape Optimization," *IEEE Transactions on Evolutionary Computation*, Vol. 4, No. 2, July 2000, pp. 182–187. doi:10.1109/4235.850658

[30] Taguchi, G., *Introduction to Quality Engineering*, Asian Productivity Organization, Tokyo, 1986.

[31] Kleijnen, J., Sanchez, S., Lucas, T., and Cioppa, T., "State-of-the-Art Review: A User's Guide to the Brave New World of Designing Simulation Experiments," *INFORMS Journal on Computing*, Vol. 17, No. 3, 2005, pp. 263–289. doi:10.1287/ijoc.1050.0136

[32] Jakeman, J., "Techniques of Sensitivity Assessment," Australian National Univ., Rept. PHY3038, Canberra, Australia, 2005.

[33] Projet N3S-Natur, Manuel Theorique, Software Package, Ver. 1.4, Simulog, Cannes, France, 2001.

[34] Ravet, F., Baudoin, C., and Schultz, J., "Modélisation Numérique des Écoulements Réactifs dans les Foyers de Turboréacteurs," *Progress in Energy and Combustion Science*, Vol. 36, No. 1, 1996, pp. 5–16.

[35] Ravet, F., and Vervisch, L., "Modeling Nonpremixed Turbulent Combustion in Aeronautical Engines Using PDF-Generator," 36th Aerospace Sciences Meeting and Exhibit, AIAA Paper 1998-1027, Jan. 1998.

[36] Townsend, J., Samareh, J., Weston, R., and Zorumski, W., "Integration of a CAD System into an MDO Framework," NASA Langley Research Center TM-207672, Hampton, VA, May 1998.

[37] Alonso, J., Martins, J., Reuther, J., Haimes, R., and Crawford, C., "High-Fidelity Aero-Structural Design Using a Parametric CAD-Based Model," 16th AIAA Computational Fluid Dynamics Conference, AIAA Paper 2003-3429, 2003.

[38] Nemec, M., Aftosmis, M., and Pulliam, T., "CAD-Based Aerodynamic Design of Complex Configurations Using a Cartesian Method," 42nd AIAA Aerospace Sciences Meeting, AIAA Paper 2004-0113, Jan. 2004.

[39] Haimes, R., "CAPRI: Computational Analysis Programming Interface. A Solid Modeling Based Infra-Structure for Engineering Analysis and Design. Rev. 2.0," Massachusetts Inst. of Technology, Cambridge, MA, Dec. 2004.

[40] Fudge, D., Zingg, D., and Haimes, R., "A CAD-Free and a CAD-Based Geometry Control System for Aerodynamic Shape Optimization," 43rd AIAA Aerospace Sciences Meeting and Exhibit, AIAA Paper 2005-0451, Jan. 2005.

[41] Allaire, G., *Analyse Numérique et Optimisation*, Ellipses, Paris, 2005.

[42] Batina, J., "Unsteady Euler Airfoil Solution Using Unstructured Dynamic Meshes," 27th AIAA Aerospace Sciences Meeting, AIAA Paper 198900115, Jan. 1989.

[43] Singh, K., Newman, J., and Baysal, O., "Dynamic Unstructured Method for Flows Past Multiple Objects in Relative Motion," *AIAA Journal*, Vol. 33, No. 4, 1995, pp. 641–649. doi:10.2514/3.12439

[44] Degand, C., and Farhat, C., "A Three-Dimensional Torsional Spring Analogy Method for Unstructured Dynamic Meshes," *Computers and Structures*, Vol. 80, Nos. 3-4, 2002, pp. 305–316. doi:10.1016/S0045-7949(02)00002-0

[45] Mohammadi, B., and Pironneau, O., *Applied Shape Optimization for Fluids*, Oxford Science, Oxford, 2001.

[46] Xiong, Y., Moscinski, M., Frontera, M., and Yin, S., "Multidisciplinary Design Optimization of Aircraft Combustor Structure: An Industry Application," *AIAA Journal*, Vol. 43, No. 9, Sept. 2005, pp. 2008–2014. doi:10.2514/1.7674

[47] Pegemanyfar, N., Pfitzner, M., and Surace, M., "Automated CFD Analysis Within the Preliminary Combustor Design System PRECODES Utilizing Improved Cooling Models," ASME Turbo Expo 2007, American Society of Mechanical Engineers Paper 2007-27409, May 2007.

[48] Shelley, J., Giullian, N., and Jensen, C., "Incorporating Computational Fluid Dynamics into the Preliminary Design Cycle," *Computer-Aided Design and Applications*, Vol. 4, No. 1-7, 2007, pp. 235–245.

[49] Buis, S., Piacentini, A., and Déclat, D., "PALM: A Computational Framework for Assembling High Performance Computing Applications," *Concurrency and Computation*, Vol. 18, No. 2, 2006, pp. 231–245. doi:10.1002/cpe.914

[50] GAMBIT, Software Package, Ver. 2.4, Fluent, Inc., Lebanon, NH, May 2007.

[51] Duchaine, F., "Optimisation de Forme Multi-Objectif sur Machines Parallèles avec Méta-Modèles et Coupleurs. Application aux Chambres de Combustion Aéronautiques," Ph.D. Thesis, Inst. National Polytechnique de Toulouse, Toulouse, France, Nov. 2007.

[52] Pareto, V., *Manuale di Economia Politica*, Piccola Biblioteca Scientifica, Milan, 1906.

[53] Patterson, H., "The Errors of Lattice Sampling," *Journal of the Royal Statistical Society Series B (Methodological)*, Vol. 16, 1954, pp. 140–149.

[54] Simpson, T., Mauery, T., Korte, J., and Misree, F., "Comparison of Response Surface and Kriging Models for Multidisciplinary Design Optimization," *7th AIAA/USAF/NASA/ISSMO Symposium on Multidisciplinary Analysis and Optimization*, Vol. 1, AIAA, Reston, VA, Sept. 1998, pp. 381–391; also AIAA Paper 1998-4755.

[55] Jin, Y., Olhofer, M., and Sendhoff, B., "On Evolutionary Optimisation with Approximate Fitness Functions," *Proceedings of the Genetic and Evolutionary Computation Conference GECCO*, Morgan Kaufmann, San Francisco, July 2000, pp. 786–793.

[56] Ong, Y., Nair, P., and Keane, A., "Evolutionary Optimization of Computationally Expensive Problems via Surrogate Modeling," *AIAA Journal*, Vol. 41, No. 4, 2003, pp. 687–696. doi:10.2514/2.1999

[57] Büche, D., Schraudolph, N., and Koumoutsakos, P., "Accelerating Evolutionary Algorithms with Gaussian Process Fitness Function Models," *IEEE Transactions on Systems, Man, and Cybernetics*, Pt. C, Vol. 35, No. 2, 2005, pp. 183–194. doi:10.1109/TSMCC.2004.841917

[58] Sasena, M., "Flexibility and Efficiency Enhancements for Constrained Global Design Optimization with Kriging Approximations," Ph.D. Thesis, Univ. of Michigan, Ann Arbor, MI, 2002.

[59] Jones, D., "A Taxonomy of Global Optimization Methods Based on Response Surfaces," *Journal of Global Optimization*, Vol. 21, No. 4, 2001, pp. 345–383. doi:10.1023/A:1012771025575

[60] MacKay, D., "Gaussian Processes: A Replacement for Supervised Neural Networks?" 1997, http://www.cs.toronto.edu/~mackay/abstracts/gp.html

[61] Byrd, R. H., Lu, P., Nocedal, J., and Zhu, C., "A Limited Memory Algorithm for Bound Constrained Optimization," *SIAM Journal on Scientific Computing*, Vol. 16, No. 5, 1995, pp. 1190–1208. doi:10.1137/0916069

[62] Zitzler, E., Deb, K., and Thiele, L., "Comparison of Multiobjective Evolutionary Algorithms: Empirical Results," *Evolutionary Computation*, Vol. 8, No. 2, 2000, pp. 173–195. doi:10.1162/106365600568202

[63] Deb, K., Pratap, A., Agarwal, S., and Meyrivan, T., "A Fast and Elitist Multi-Objective Genetic Algorithm : NSGA-II," *IEEE Transactions on Evolutionary Computation*, Vol. 6, No. 2, Apr. 2002, pp. 182–197. doi:10.1109/4235.996017

[64] Goldberg, D., *Genetic Algorithms in Search, Optimization and Machine Learning*, Addison–Wesley, Boston, 1989.

[65] Forrester, A., "Efficient Global Aerodynamic Optimisation Using Expensive Computational Fluid Dynamics Simulations," Ph.D. Thesis, Univ. of Southampton, School of Engineering Sciences, Southampton, England, U.K., Nov. 2004.

[66] Forrester, A., Sobester, A., and Keane, A., "Optimization with Missing Data," *Proceedings of the Royal Society of London, Series A: Mathematical and Physical Sciences*, Vol. 462, No. 2067, 2006, pp. 935–945. doi:10.1098/rspa.2005.1608

[67] Joseph, V., and Hung, Y., "Orthogonal Maximin Latin Hypercube Designs," *Statistica Sinica*, Vol. 18, No. 1, 2008, pp. 171–186.

[68] Chen, V., Tsui, K., Barton, R., and Meckesheimer, M., "A Review on Design, Modeling and Applications of Computer Experiments," *IIE Transactions*, Vol. 38, Apr. 2006, pp. 273–291. doi:10.1080/07408170500232495

[69] Meckesheimer, M., "A Framework for Metamodel-Based Design: Susbsystem Metamodel Assessment and Implementation Issues," Ph.D. Thesis, Pennsylvania State Univ., University Park, PA, 2001.

[70] Lefebvre, A., *Gas Turbines Combustion*, Taylor and Francis, Philadelphia, 1999.

[71] Morris, M., "Factorial Sampling Plans for Preliminary Computational Experiments," *Technometrics*, Vol. 33, No. 2, 1991, pp. 161–174. doi:10.2307/1269043

[72] Campolongo, F., Cariboni, J., Saltelli, A., and Schoutens, W., "Enhancing the Morris Method," *4th International Conference on Sensitivity Analysis of Model Output (SAMO)*, edited by K. Hanson and F. Hemez, Elsevier, Oxford, 2004, pp. 369–379.

[73] Saltelli, A., *Global Sensitivity Analysis*, Wiley, Hoboken, NJ, 2007.

T. Zang
Associate Editor